energies

MDPI

Article

The Application of Tuned Inductors in Electric Power Systems

Michał Gwóźdź

Faculty of Control, Robotics and Electrical Engineering, Poznan University of Technology, Piotrowo 3A Street, 60-965 Poznan, Poland; michal.gwozdz@put.poznan.pl

Abstract: This work focuses on the possibility of using a tuned inductor in electric power systems with adaptive features. The presented idea of inductor operation, using an interaction of the magnetic fluxes, is a new approach to designing such devices. Examples of power adaptive systems are devices for improving the quality of electricity. Therefore, various types of 'compensators' of reactive power (or both reactive and distortion power) are used in electrical systems as a preventive measure. The tuned inductor, presented in this work, offers wider possibilities for power compensation in electric systems, compared to the classic solutions of compensators based on fixed inductors. Another possible implementation of such an inductor solution is in static power electronic devices, installed in AC transmission grids to increase power transfer capability, stability, and controllability, through a series and/or shunt compensation. Nevertheless, the use of the proposed device in the aforementioned electric systems is only one example of the possible implementations in the power electronics area. In this work, the following issues are presented: exemplary solutions of compensators with the adaptive features, rules of the tuned inductor operation, test results of the 3D field model of the inductor, and test results of the laboratory model of the electric system with this device.

Keywords: adaptive compensator; converter control; quality of electricity; tunable inductive filter

Citation: Gwóźdź, M. The Application of Tuned Inductors in Electric Power Systems. *Energies* **2022**, *15*, 8481. https://doi.org/10.3390/en15228481

Academic Editors: Ralph Kennel and Mohamed Abdelrahem

Received: 22 October 2022
Accepted: 10 November 2022
Published: 13 November 2022

1. Introduction

This work focuses on the idea of the operation, and possible implementation, of a tuned inductor (TI) in power electronics systems with adaptive features. The first large group of such devices comprises systems for improving the quality of electrical energy [1–4]. The second possible area of implementation of the tuned inductor solution is static power-electronic systems installed in AC transmission grids, to increase their power transfer capability, stability, and controllability, through series and/or shunt compensation, known as the Flexible AC Transmission Systems (FACTS) [1,5,6]. The third area concerns AC/DC and DC/DC converters, allowing shaping of the frequency characteristics of these devices [7–10]. Nevertheless, this work focuses on the application of the tuned inductor in the first group of aforementioned power systems.

The negative effect of non-linear loads on the operation of the power line, resulting in lowering the desired values of parameters of electric energy [11], is a widely known and well-documented phenomenon. Therefore, various types of 'compensators', mainly different kinds of power filters, are used in the electrical systems as a preventive measure [1,12–14]. The main task of these devices is appropriate matching of the current's shape at its input to the shape of a current, drawn from the same grid node by other loads. As a result of such a 'compensation process', the current, flowing from the power line to the load, should have both suitable shape and right phase relation with the voltage in the power line node. This process depends on the chosen compensation strategy, relative to only reactive power or also the distortion power [2,15–17].

The presented idea of the tuned inductor operation is a new approach to the design of power devices with the adaptive compensation feature. However, in relation to this work, the operation of the adaptive compensator, as a whole, is not related to any specific power

theory. Moreover, using the inductor in such devices is only one example of its possible implementations in the field of electric power systems.

This paper contains five sections, which cover the following issues: exemplary topology of the adaptive compensator in a passive and active version, basics of operation of the tuned inductor, investigations of the inductor magnetic simulation model, test results of the laboratory prototype of the electric power system with the inductor, and conclusions.

2. Adaptive Devices for Improving the Quality of Electricity

2.1. Passive Compensator

The fixed parameters compensator improves the power factor of a supply source when its load also has fixed parameters. When these parameters are not constant, the effectiveness of a such compensator operation is lost [1,3,13,18], so an adaptive compensator is needed instead. A reactive compensator has adaptive properties if it can be adjusted to changes in the load power. This can be carried out by switches or by using reactive elements with controllable parameters. Adaptive compensators can be built as reactive compensators with semi-controlled devices, such as thyristors, or as switching compensators, commonly known as active power filters (APF), which use different types of transistors in the compensator's power stage. When the load powers are very high, as this is common for large manufacturing plants, the APFs are not usually sufficient in such applications, however.

A block diagram of an exemplary electric system with a generalised passive compensator (PC) [1,3,13] is shown in Figure 1a.

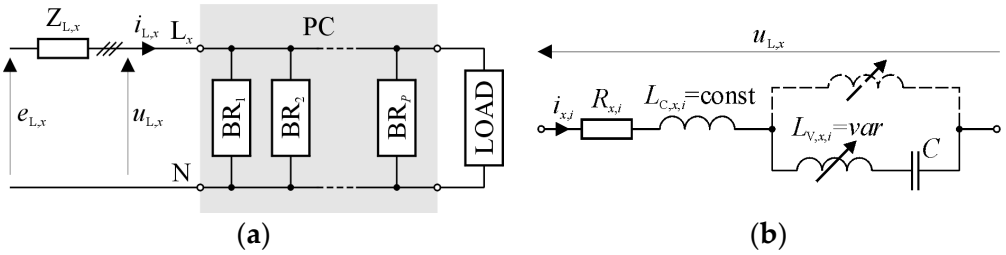

Figure 1. Block diagram of the passive adaptive compensator (**a**) and the diagram of its single branch (**b**).

The PC contains P individual branches ($BR_i : i = 1,\ 2,\ \ldots\ ,\ P$) that can be connected in a different manner, e.g., in parallel, as shown in Figure 1a. The exemplary topology of the single branch, using the tuned inductors, is shown in Figure 1b. As a result, the impedance of this circuit can vary:

$$\underline{Z_{x,i}} = \frac{\underline{U_{L,x}}}{\underline{I_{L,x}}} = \text{var} : x = 1,\ 2,\ 3, \tag{1}$$

where x is the phase number in the power line.

However, it should be stated that this device is not, formally, a fully passive compensator, as it follows from its scheme, because the 'passive' compensator also contains power electronics components. These devices are necessary for controlling the tuned inductor; their role in this system is explained in Section 3.

2.2. Shunt Active Power Filter

The topology of the 1-phase electric system, containing a shunt active power filter (SAPF), is shown in Figure 2. The SAPF is included between the power line and the nonlinear load (NL).

A typical filter of this type consists of the following, basic elements [1–3]:

- Voltage source inverter (VSI), with the inductive filter (L_{CS}), included at its output;
- Reference signal generator (RSG);
- Current transducers (CT1 and CT2).

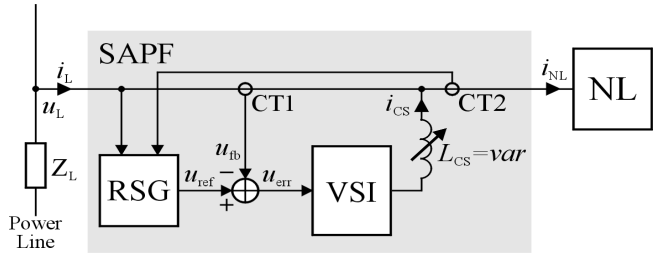

Figure 2. Block diagram of the electric system with the shunt active power filter.

The VSI and inductive filter made up the power electronics voltage-controlled current source (VCCS). Respecting the assumed functions of the VCCS in the SAPF, the role of the inductive filter is twofold; it increases the output impedance of the current source and minimises the magnitude of its input (or output) current component, associated with PWM (or other kinds of pulse modulation) [1]. Taking into account the SAPF topology [1–3], the VCCS has the highest dynamics (i.e., the 'frequency response') when the instantaneous value of the power line voltage passes through zero, whereas when this voltage reaches the maximum value, the value of dynamics is lowest. Since both the value of the power line voltage and the voltage in the DC link of the VSI are set in advance, the most important treatment that can enlarge the 'frequency response' of the current source is lowering the value of the inductive filter inductance. Unfortunately, this will result also in an increase in the magnitude of the pulse modulation carrier component in the SAPF input (i.e., power line) current (i_L). Hence, in order to increase the dynamics of the VCCS, the use of an inductive filter (reactor) with a variable inductance value was proposed. This solution allowed for a better approximation of the waveform (i.e., its shape) of the SAPF input current to the reference signal (u_{ref}) waveform, in situations of highly dynamic changes in the nonlinear load current (i_{NL}), compared to a VCCS using a fixed filter. At the same time, in the steady states of operation of the SAPF, the magnitude of the PWM carrier component in its input current stays at the minimum assumed level. The details of the concept of such VCCS operating, filter design procedure (in its preliminary version), and results of its laboratory model tests, were presented in the previous work [19].

3. Idea of Operation of the Tuned Inductor

For the implementation of an inductor with a variable inductance feature, a circuit with magnetically coupled coils (forming a kind of transformer) was used, see Figure 3.

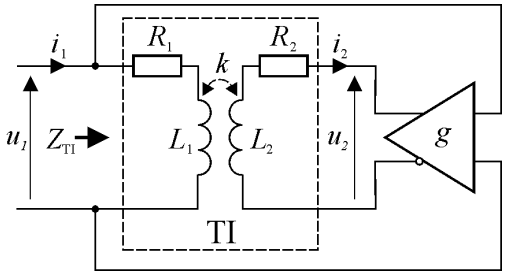

Figure 3. Principle of operation of the tuned inductor.

The circuit consists of two main elements. The first of these is the aforementioned transformer (TI block), equipped with an air-gap in the magnetic core; the width of the air-gap influences the value of the magnetic coupling factor (k). The second element is the differential power electronics amplifier, with a gain factor about equal to g, which powers the secondary coil of the transformer. The resultant magnetic flux in the core of the transformer can be amplified or weakened, which also results in a change in the equivalent impedance ($\underline{Z_{TI}} = R_{TI} + jX_{TI}$) of this circuit when seen from the power source (u_1) side. The

value of this impedance depends on the values of the parameters in the circuit, especially k and g factors.

The calculation of the value of the equivalent impedance is based on the analysis, using the basic properties of magnetically coupled circuits. The initial assumptions made do not take into account the nonlinearity of the magnetic core, on which the coils are wound, and the voltage's excitation (u_1) was sinusoidal. The equations, describing the voltage and current relations in this circuit, are as follows:

$$\underline{U_1} = R_1\underline{I_1} + \mathrm{j}X_1\underline{I_1} + \mathrm{j}X_\mathrm{M}\underline{I_2}, \tag{2}$$

$$\underline{U_2} = R_2\underline{I_2} + \mathrm{j}X_2\underline{I_2} + \mathrm{j}X_\mathrm{M}\underline{I_1}, \tag{3}$$

where: X_1, X_2, and X_M are the self and mutual reactance of the coils, respectively.

Taking $\underline{U_2} = g\underline{U_1}$ into account (where $0 \leq g \leq 1$), as a result of the transformations of Equations (2) and (3), the following formula was obtained, defining the value of the equivalent impedance of the circuit:

$$\underline{Z_\mathrm{TI}} = \frac{\underline{U_1}}{\underline{I_1}} = \frac{R_1 + \mathrm{j}X_1 + \frac{X_\mathrm{M}^2}{R_2 + \mathrm{j}X_2}}{1 - \mathrm{j}g\frac{X_\mathrm{M}^2}{R_2 + \mathrm{j}X_2}}, \tag{4}$$

in which:

$$X_\mathrm{M} = k\sqrt{X_1X_2}, \tag{5}$$

where $0 \leq k \leq 1$.

Considering Equations (4) and (5), the equation making the value of Z_TI dependent on the other parameters of the circuit is as follows:

$$\underline{Z_\mathrm{TI}} = \frac{\underline{U_1}}{\underline{I_1}} = \frac{R_1 + \mathrm{j}X_1 + k^2\frac{X_1X_2}{R_2 + \mathrm{j}X_2}}{1 - \mathrm{j}gk\frac{\sqrt{X_1X_2}}{R_2 + \mathrm{j}X_2}}. \tag{6}$$

For the extraction of the X_TI component of Equation (6), both resistances were omitted. In such a case, Equation (6) takes the following form:

$$X_\mathrm{TI} = \frac{1 - k^2}{1 - gk\sqrt{\frac{X_1}{X_2}}}X_1. \tag{7}$$

Assuming then the equality of both of the reactances (i.e., $X_1 = X_2 = X$), Equation (7) takes the final form:

$$X_\mathrm{TI} = \frac{1 - k^2}{1 - gk}X. \tag{8}$$

Based on Equation (8), by changing the value of the gain factor (g), it is possible to achieve the value of X_TI, in the range:

$$\left(1 - k^2\right)X \leq X_\mathrm{TI} \leq (1 + k)X. \tag{9}$$

The graphic visualisation of Equation (8), as a value of X_TI, in relation to X, vs. g, while k = const, is shown in Figure 4.

This relationship, for small gain factor values, is almost flat. Changes in the value of X_TI become more visible for the gain's value greater than 0.6.

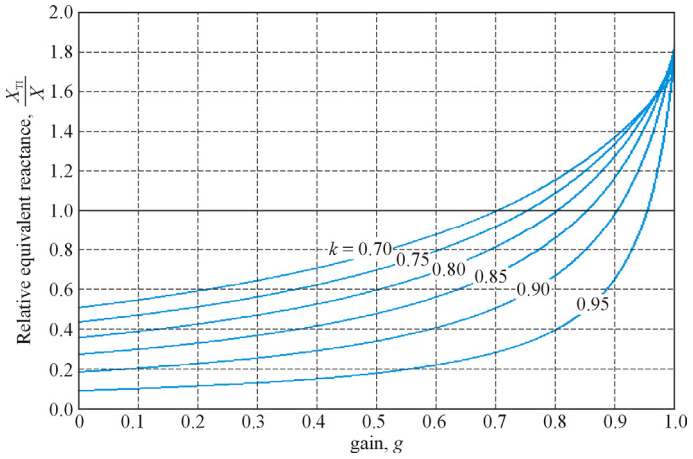

Figure 4. Curves of X_{TI}, in relation to X, vs. g, while k = const.

4. Inductor's Field Simulation Model Studies

The aim of this research was to obtain the technical details of the inductor, necessary for the design of a laboratory prototype. The simulation studies of the tuned inductor field model were conducted using optimisation software and the Maxwell Environment [20]. This study found that, to achieve the assumed value of the inductance of the TI, a sophisticated design of its magnetic circuit is necessary. As a result, the three-column magnetic core was selected for the transformer. The primary coil was wound on the central column of the device, while the secondary coil was divided and wound on the two external columns. In order to achieve the assumed effect of the transformer operation, through the possibility of changing the equivalent inductance, the secondary coils should be properly interconnected. To simplify the modelling process, it was also assumed that the number of turns of all three coils would be equal to each other, i.e., $z_1 = z_{21} = z_{22}$. The results of these preliminary tests led to the design of the tuned inductor, as shown in Figure 5.

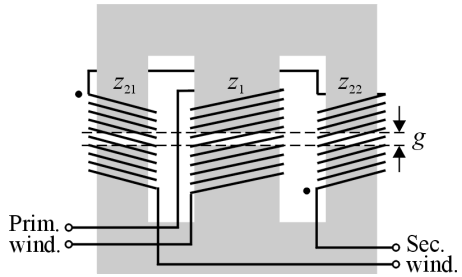

Figure 5. The technical details of the design of the tuned inductor.

Taking into account the potential fields of application of the tuned inductor based on previous work [19,21], it was assumed that: X = 4.50 mH and k = 0.80.

For the purpose of modeling the inductor, its 3D-field model was employed. In this model, the characteristics of the ferrite E-shapes (OT49928EC), made of T-type ferrite material (manufactured by MAGNETICS Inc. [22]), were used. The model of the core was composed of four E-shapes.

In order to obtain the desired parameter values (i.e., the air-gap width as well as the number of turns) in the first stage of the design process, authored software was implemented, using the Particle Swarm Optimisation (PSO) algorithm [23,24], coupled with the Magnetic Equivalent Circuit (MEC) method [25,26]. The initial optimisation of the inductor structure was carried out with the use of the MEC model. The results of these calculations, obtained for the first stage of the design process, were then used to select the solutions for which the calculated values of inductance were in the area of the expected

values. Then, as part of the second stage, the verification calculations were carried out for the values of the parameters obtained from the first stage using a 3D field model. A more in-depth optimisation of the construction of the inductor was also carried out. This time, the calculations were made in the area of selected decision variables, obtained in the first stage.

In the second stage of the design process, the Interval Search Method was used [27], implemented in the optimisation module of Maxwell Software, using the Finite Element Method (FEM). Details of the whole research procedure, as well as its results, were presented in the previous works [19,21].

A short summary of the basic parameters for the tuned inductor, achieved as a result of 3D-field simulation model studies, is as follows:

- Air gap width: g = 2.0 mm;
- Number of turns: $z_1 = z_{21} = z_{22} = 80$.

5. Laboratory Tests and Discussion

5.1. Tests of the Prototype of the Tuned Inductor

The general view of the laboratory setup is shown in Figure 6. In the power stage of the tested circuit, the P3-5-550MFE LABINVERTER [28] was implemented. This universal device was designed for applications in advanced R&D electronic power systems. The control module of the inverter comprised an ALS-G3-1369 Evaluation Board [28] with an Analog Devices Inc., ADSP-21369 SHARC® digital signal processor (DSP). This board is specialised for such electronic power applications that require, among others, the high computation power of a CPU and a precision, high resolution PWM pattern.

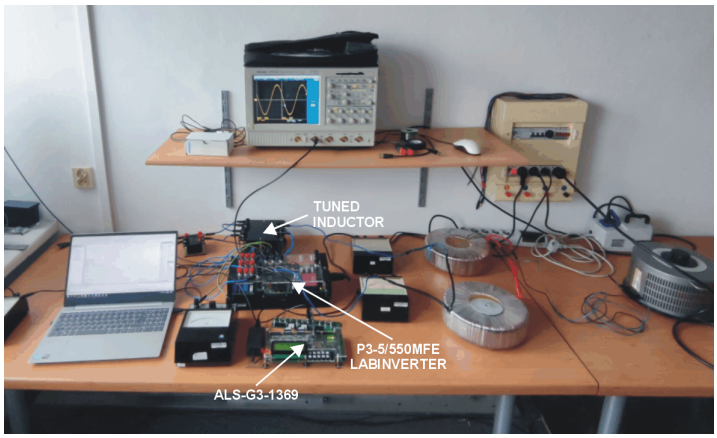

Figure 6. View of the laboratory stand.

The aim of the first part of the research was to confirm the parameters achieved for the laboratory prototype of this device in relation to the inductor's field model. The view of the inductor laboratory model is shown in Figure 7.

The inductance measurement methodology depended on the observation of voltage and current waveforms in the circuit with the tuned inductor, as shown in Figure 8. These waveforms then formed the basis for calculating the inductor inductance.

The general formula describing voltage and current waveforms in this circuit, in the time-domain, is as follows:

$$u_1(t) = R_{TI} i_1(t) + L_{TI} \frac{\mathrm{d}i_1(t)}{\mathrm{d}t}. \tag{10}$$

Disregarding the circuit's resistance for practical purposes, the formula defining the relationship of current and voltage takes the following form:

$$i_1(t) = \frac{1}{L_{\mathrm{TI}}} \int_t u_1(t) \mathrm{d}t. \tag{11}$$

Assuming that a supply voltage is a rectangular function of time, the current waveform will be a linear function of time, i.e., a first-order polynomial. As a result, the value of equivalent inductance of the TI can be calculated, based on the formula:

$$L_{\mathrm{TI}} = \frac{\Delta u_1}{\Delta i_1} \Delta t, \tag{12}$$

where: Δu_1, Δi_1, and Δt are the growth in the voltage, current, and time value, respectively.

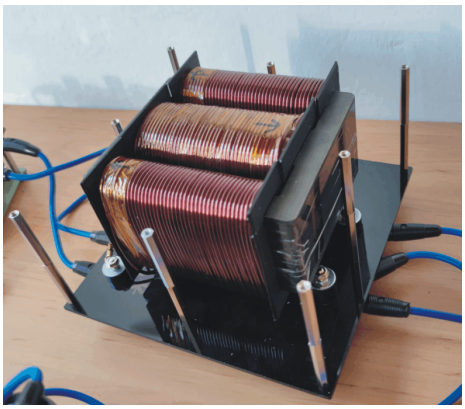

Figure 7. General view of the laboratory prototype of the tuned inductor.

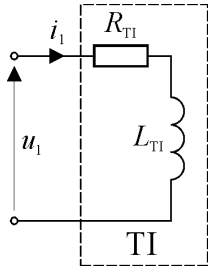

Figure 8. The measurement circuit for calculating the TI inductance.

The graphic visualisation of the measurement methodology, based on Equation (12), is shown in Figure 9, where T_t is the period of voltage supply.

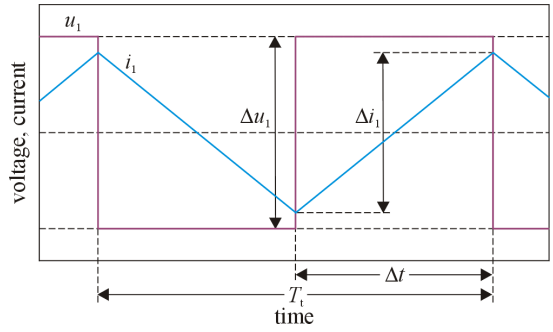

Figure 9. Curves of voltage and current in the measurement circuit, as a visualisation of (11).

The assumption was made that omitting the TI resistance does not result in a significant value of error when calculating the inductance value, under the condition that the measurement time (Δt) is much shorter than the circuit time constant, i.e.:

$$\Delta t << \frac{L_{TI}}{R_{TI}}. \tag{13}$$

The laboratory setup consisted of the following elements: tested inductor (TI), DC power supply, power electronics inverter (VSI), operating as the generator of the measurement circuit supply voltage, and inverter control system. As the VSI, the aforementioned laboratory inverter (P3-5.0/550MFE) was used, with an ALS-G3-1369 Evaluation Board as the control module.

The measurement methodology was based on supplying the primary coil of TI with the voltage (u_1) around a rectangular shape. Then, this voltage and primary current (i_1) were observed and registered with the aid of a TDS3054 oscilloscope. This methodology allowed for the use of a large current in this circuit. As a result, observation of the saturation state of the core was also possible. However, the inductance measurements were related to the quasi-linear operating range of the core. During testing, the voltage and current waveforms were periodic signals; the value of fundamental frequency u_1 was fixed and set at 500 Hz.

Figure 10 presents the characteristic waveforms in the measurement circuit during the laboratory tests.

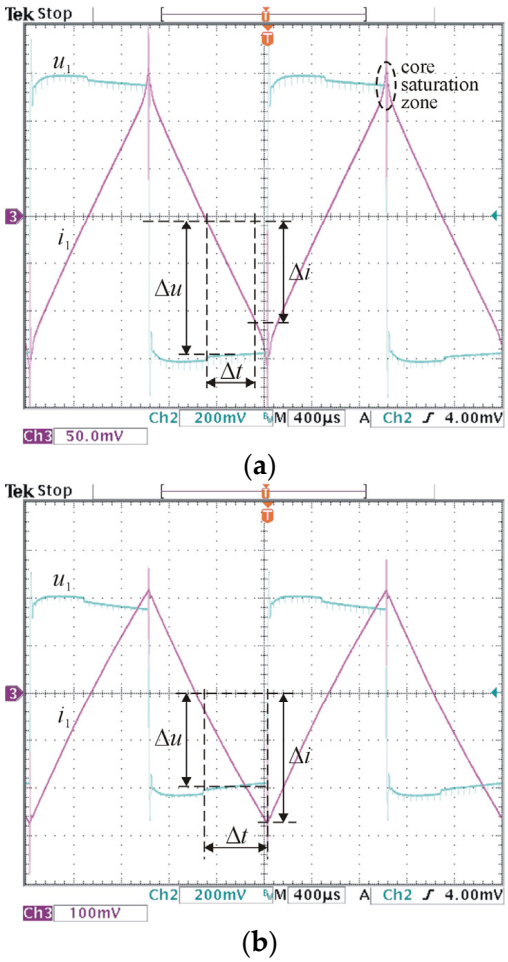

Figure 10. Waveforms of primary voltage and current in the primary coil of the inductor, while its secondary coil was: (**a**) open, (**b**) short-circuited. Vertical scale: (**a**) 40 V/div, 5 A/div, (**b**) 40 V/div, 10 A/div.

As a result of laboratory investigations, the following values of the inductor parameters were obtained:

- Number of turns: $z_1 = z_{21} = z_{22} = 80$;
- Air gap width: $g = 2.0$ mm;
- Inductance (in the quasi-linear range of the magnetic core operation), secondary coil open: $L_{TI} = 4.3$ mH;
- Inductance (in the quasi-linear range of the magnetic core operation), secondary coil closed: $L_{TI} = 1.6$ mH;
- Coil resistance: $R_1 = 110$ mΩ, $R_2 = 220$ mΩ.
- Thus, taking into account all of the aforementioned assumptions related to the tuned inductor model and taking into account the test results, the calculated value of the coupling factor $k = 0.79$.

5.2. Tests of the Electric System with a Tuned Inductor

The block scheme of the circuit, used for testing the tuned inductor operation, is shown in Figure 11.

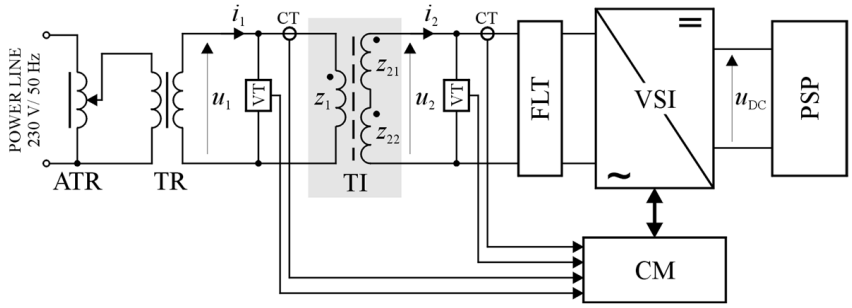

Figure 11. Block scheme of the circuit, used for testing the tuned inductor.

This circuit consisted of the following main blocks:

- Isolated power line, equipped with an EMI filter at the input;
- Auto-transformer (ATR) and transformer (TR);
- Tested inductor (TI);
- Voltage source inverter (VSI);
- LCL filter (FLT), included at the output of the VSI;
- Inverter control module (CM);
- Voltage and current, isolated transducers (VT and CT);
- Regulated DC power supply (PSP).

The VSI, configured as the H-bridge, and FLT block made up the power electronics voltage-controlled voltage source (VCVS) that powered the secondary coil of the transformer.

A set of tests were conducted on the inductor using HIL (HIL—'hardware-in-the-loop') modelling. Most of the achieved waveforms were obtained using the 'PLOT' function of the VisualDSP++® environment [29]. This function allows for the easy graphic visualisation of numerical data (typically representing waveforms) stored in the objects of the C-Language, such as arrays. The compiler of the C-Language is a component part of VisualDSP++®.

Taking into account the value of the magnetic coupling coefficient achieved, the family of curves shown in Figure 4 took the form shown in Figure 12.

In Figure 12, the characteristic values of the reactance of the TI are also marked, i.e., for: $g = 0.0$, $g = k = 0.79$, and $g = 1.0$.

In turn, Figures 13–15 present characteristic waveforms of the voltages and currents (u_1, i_1, u_2, and i_2). During tests, the RMS value of the power supply (u_1) was set at 18 V.

In turn, the system response to a step change in the value of gain factor of the power amplifier (in the range $0.05 \div 0.95$) is shown in Figure 16.

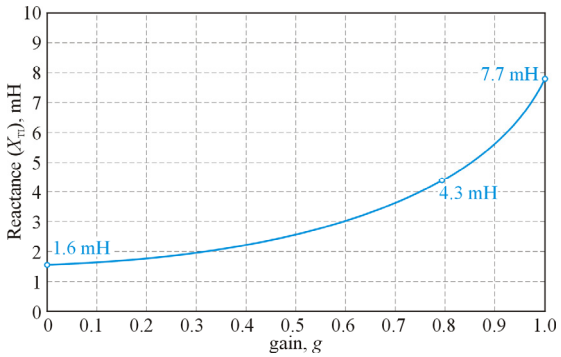

Figure 12. Curve of X_{TI} vs. g, where k = 0.79.

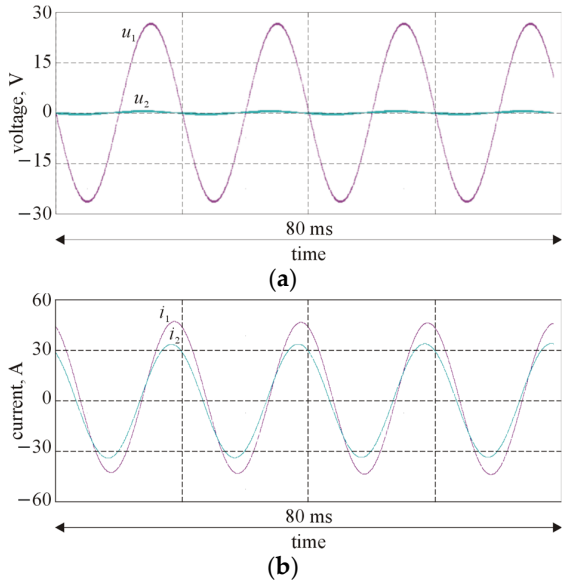

Figure 13. Waveforms of voltage (**a**) and current (**b**) in the primary and secondary winding of the TI for the gain coefficient: g = 0.0.

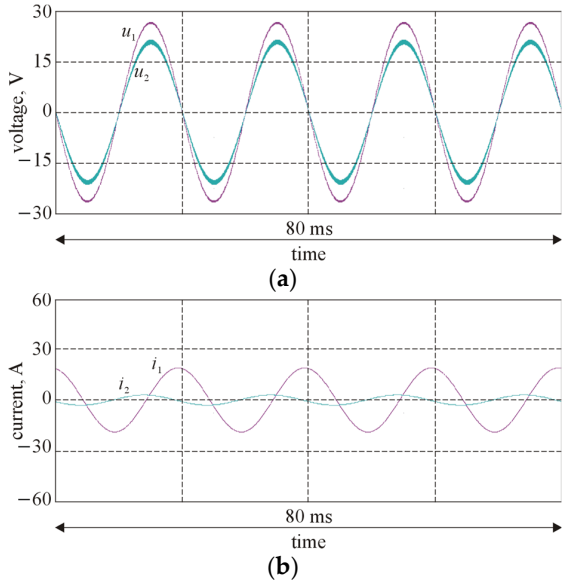

Figure 14. Waveforms of voltage (**a**) and current (**b**) in the primary and secondary winding of the TI for the gain coefficient: g = 0.79.

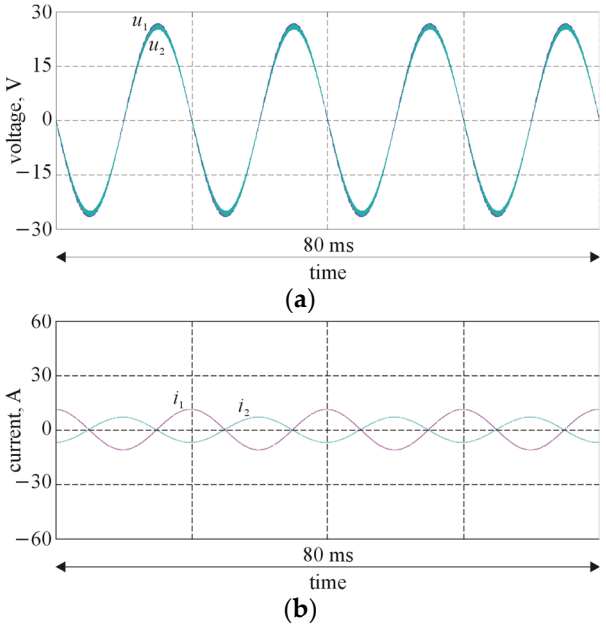

Figure 15. Waveforms of voltage (**a**) and current (**b**) in the primary and secondary winding of the TI for the gain coefficient: g = 1.0.

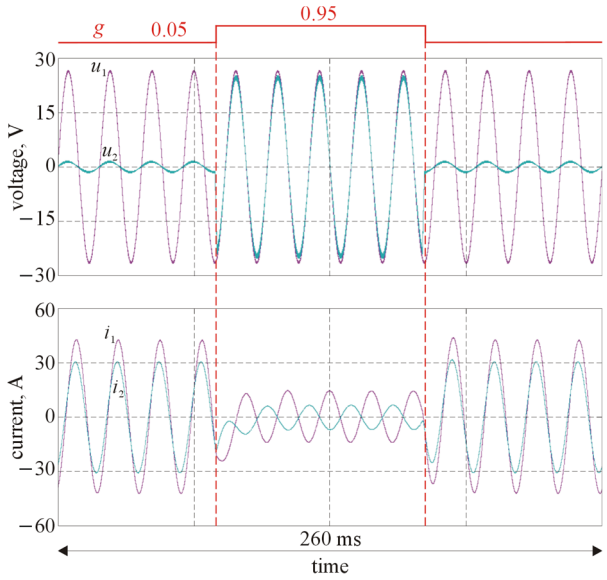

Figure 16. System response to a step change in the value of g.

5.3. Discussion of the Test Results

As the test results show, the current amplitude in the primary and secondary circuits of the transformer changes with the change in value of the gain coefficient. However, the actual values of the equivalent inductance of TI differ from the theoretical assumptions, given by Equation (6); they are affected by an error in the range 7.8 ÷ 14.3%. The error value increases as the gain factor decreases, which results in a decrease in the equivalent reactance of the TI. This error is the result of factors such as: the presence of resistance in the real circuit, the difference between the theoretical and actual voltage value in the secondary circuit of the transformer (caused by the gain error of the power amplifier), and the presence of a ripple component in this voltage, caused by the pulse-width modulation (PWM) used to control the inverter (VSI). Furthermore, the phase relationship of the primary and secondary currents also changes. The primary current phase shift from the

supply voltage is less than desired (i.e., 90°) because the circuit contains the aforementioned 'parasitic' resistances, including R_1, and R_2, etc. The value of this phase shift mainly results from Equation (8). However, this equation does not take into account all elements which were contained the real circuit (e.g., resistance and reactance of the power line).

Testing of the system's impulse response to a step change in the gain value allowed for the assessment of values of its dynamic parameters, which depended on the actual value of reactance of the TI. In relation to Figure 16, the durations of the transient states in the circuit were equal to approximately 35 ms, on average.

6. Conclusions

This work presents the principles of operation and the test results for the simulation and laboratory models of an electric system with a variable inductance reactor. The idea of the reactor operation was based on coupled fluxes, but without using the natural nonlinearity of the magnetic circuit, as in most of the previous studies, e.g., ref. [30]. Instead, the interaction of two magnetic fluxes was implemented in the ferromagnetic core. The investigation results confirmed the possibility of obtaining the inductance values required in a smooth manner, as a result of controlling the flux in the inductor with three coils (wound on the three-legged magnetic core) with relative error values in the range 7.8 ÷ 14.3%. In the author's opinion, this value can be considered satisfactory, taking into account the high complexity of both the magnetic circuit of the device and the entire system with the reactor. An additional advantage of the presented circuit with a TI is that the apparent power of the inverter supplying the secondary coil of the transformer can be an average of *k*–times lower than the power of the primary circuit.

Whereas, in the current stage of this research, phenomena related to power loss in the tuned reactor were not analysed.

In the author's opinion, the device presented in this work can be an attractive solution, especially in electric power systems with adaptive features, including devices for improving an energy quality and systems for energy transmission. However, these applications of the tuned inductor need further investigations, through simulation models and laboratory prototypes.

Funding: This research was funded by Poznan University of Technology, grant number: SBAD 0567/2022.

Data Availability Statement: Not applicable.

Conflicts of Interest: The author declare no conflict of interest.

References

1. Rashid, M.H. *Power Electronics Handbook*; Elsevier Ltd.: Oxford, UK, 2018.
2. Akagi, H.; Watanabe, E.H.; Aredes, M. *Instantaneous Power Theory and Applications to Power Conditioning*; John Wiley & Sons: Hoboken, NJ, USA, 2017; ISBN 9781118362105.
3. Pasko, M.; Buła, D.; Dębowski, K.; Grabowski, D.; Maciążek, M. Selected methods for improving operating conditions of three-phase systems working in the presence of current and voltage deformation—Part I. *Arch. Electr. Eng.* **2018**, *67*, 591–602. [CrossRef]
4. Trinh, Q.; Lee, H. An enhanced grid current compensator for grid-connected distributed generation under nonlinear loads and grid voltage distortions. *IEEE Trans. Ind. Electron.* **2014**, *61*, 6528–6537. [CrossRef]
5. Hamdy, M.; Abdelaziz, A.Y.; Ray, P.; Attia, M.A. Comparison between flexible AC transmission systems (FACTs) and filters regarding renewable energy systems harmonics mitigation. *Int. J. Emerg. Electr. Power Syst.* **2021**, *23*, 211–220. [CrossRef]
6. Benchabira, A.; Khiat, M. A hybrid method for the optimal reactive power dispatch and the control of voltages in an electrical energy network. *Arch. Electr. Eng.* **2019**, *68*, 535–551.
7. Yang, Y.; Ma, J.; Ho, C.; Zou, Y. A new coupled-inductor structure for interleaving bidirectional dc-dc converters. *IEEE J. Emerg. Sel. Top. Power Electron.* **2015**, *3*, 841–849. [CrossRef]
8. Yang, C.; Liu, Y.; Tseng, P.; Pan, T.; Chiu, H.; Lo, Y. DSP-Based Interleaved Buck Power Factor Corrector With Adaptive Slope Compensation. *IEEE Trans. Ind. Electron.* **2015**, *62*, 4665–4677. [CrossRef]
9. Onal, Y.; Sozer, Y. Bridgeless SEPIC PFC converter for low total harmonic distortion and high power factor. In Proceedings of the Applied Power Electronics Conference and Exposition (APEC), Long Beach, CA, USA, 20–24 March 2016; pp. 2693–2699.

10. Liu, J.; Xu, W.; Chan, K.W.; Liu, M.; Zhang, X.; Chan, N.H.L. A Three-Phase Single-Stage AC–DC Wireless-Power-Transfer Converter With Power Factor Correction and Bus Voltage Control. *IEEE J. Emerg. Sel. Top. Power Electron.* **2020**, *8*, 1782–1800. [CrossRef]
11. Masetti, C. Revision of European Standard EN 50160 on power quality: Reasons and solutions. In Proceedings of the 14th International Conference on Harmonics and Quality of Power-ICHQP, Bergamo, Italy, 26–29 September 2010.
12. Popescu, M.; Bitoleanu, A.; Linca, M.; Suru, C.V. Improving Power Quality by a Four-Wire Shunt Active Power Filter: A Case Study. *Energies* **2021**, *14*, 1951. [CrossRef]
13. Czarnecki, L.; Almousa, M. Adaptive balancing by reactive compensators of three-phase linear loads supplied by nonsinusoidal voltage from four-wire lines. *Am. J. Electr. Power Energy Syst.* **2021**, *10*, 32–42. [CrossRef]
14. Ye, T.; Dai, N.; Zhu, M. Optimise the series LC design of a quasi-proportional-resonant controlled hybrid active power filter for harmonic compensation. In Proceedings of the 11th Conference on Industrial Electronics and Applications (IEEE ICIEA), Hefei, China, 5–7 June 2016; pp. 624–629. [CrossRef]
15. Depenbrock, M.; Marshal, D.A.; Wyk, J.D. Formulating requirements for universally applicable power theory as control algorithm in power compensators. *Eur. Trans. Elect. Power ETEP* **1994**, *4*, 445–456. [CrossRef]
16. Qiao, X.; Bian, J.; Chen, C.; Li, H. Comparison and analysis of reactive power compensation strategy in power system. In Proceedings of the IEEE Sustainable Power and Energy Conference (IEEE iSPEC), Beijing, China, 21–23 November 2019; pp. 689–692. [CrossRef]
17. Benysek, G.; Pasko, M. (Eds.) *Power Theories for Improved Power Quality*; Springer-Verlag: London, UK, 2012.
18. Lee, Y.; Song, H. A Reactive power compensation strategy for voltage stability challenges in the Korean power system with dynamic loads. *Sustainability* **2019**, *11*, 326. [CrossRef]
19. Ciepliński, Ł.; Gwóźdź, M.; Wojciechowski, R.M. Application of a Tuned Inductor in a DC Power Supply with an Active Compensation Function. *Energies* **2022**, *15*, 6108. [CrossRef]
20. ANSYS Software. Available online: https://www.ansys.com/products/electronics/ansys-maxwell (accessed on 5 October 2022).
21. Gwóźdź, M.; Wojciechowski, R.M. Use of the tuned multi-legs inductor in the device for improving a quality of electric energy. In Proceedings of the LV Symposium on Electrical Machines—SME, Poznań, Poland, 27–28 April 2022; pp. 1–2.
22. MAGNETICS Inc. Available online: https://www.mag-inc.com/home (accessed on 5 October 2022).
23. Knypiński, Ł.; Nowak, L.; Demenko, A. Optimisation of the synchronous motor with hybrid permanent magnet excitation system. *COMPEL* **2015**, *34*, 448–4552. [CrossRef]
24. Devarapalli, R.; Sinha, N.K.; Venkateswara Rao, B.; Knypiński, Ł.; Naga Lakshmi, N.J.; Márquez, F.P.G. Allocation of real power generation based on computing over all generation cost: An approach of salp swarm algorithm. *Arch. Electr. Eng.* **2021**, *70*, 337–349. [CrossRef]
25. Balakrishnan, A.; Joines, W.; Wilson, T. Air-gap reluctance and inductance calculations for magnetic circuits using a Schwarz-Christoffel transformation. In *Proceedings of PESC '95—Power Electronics Specialist Conference*; IEEE: New York, NY, USA, 1995; Volume 2, pp. 1050–1056. [CrossRef]
26. Zhang, X.; Xiao, F.; Wang, R.; Fan, X.; Wang, H. Improved calculation method for inductance value of the air-gap inductor. In Proceedings of the 1st China International Youth Conference on Electrical Engineering (IEEE CIYCEE), Wuhan, China, 1–4 November 2020; pp. 1–6. [CrossRef]
27. Chong, E.; Zak, S. *An Introduction to Optimisation*, 4th ed.; Wiley Publishing: Indianapolis, IN, USA, 2013.
28. ALFINE-TIM. Available online: http://analog.alfine.pl/oferta/produkty-alfine/systemy-uruchomieniowe (accessed on 5 October 2022).
29. VDSP++ 5.0, Run-Time Library Manual for SHARC® Processors, Revision 1.5; January 2011, Part Number 82-000420-09, Analog Devices, Inc.: Norwood, MA, USA, One Technology Way. Available online: https://www.analog.com/media/en/dsp-documentation/software-manuals/50_21k_rtl_mn_rev_1.5.pdf (accessed on 5 October 2022).
30. Saeed, S.; Georgious, R.; Garcia, J. Modeling of magnetic elements including losses application to variable inductor. *Energies* **2020**, *13*, 1865. [CrossRef]